Biogeosciences Open Access
Discussions

Sedimentary and atmospheric sources of iron around South Georgia, Southern Ocean: a modelling perspective

I. Borrione[1], O. Aumont[2], M. C. Nielsdóttir[3,*], and R. Schlitzer[1]

[1]Alfred-Wegener-Institut, Helmholtz-Zentrum für Polar- und Meeresforschung,
Columbusstrasse, 7568 Bremerhaven, Germany
[2]Laboratoire de Physique des Océans Institut Européen de la Mer, 29280 Plouzané, France
[3]University of Southampton, National Oceanography Centre, European Way, SO14 3ZH,
Southampton, UK
[*]now at: Old Dominion University, Department of Ocean, Earth and Atmospheric Sciences,
4600 Elkhorn Avenue, Norfolk, VA 23529, USA

Correspondence to: I. Borrione (ines.borrione@awi.de)

BGD

10, 10811–10858, 2013

Sedimentary and atmospheric sources of iron around South Georgia

I. Borrione et al.

Title Page

Abstract	Introduction
Conclusions	References
Tables	Figures

I◀	▶I
◀	▶
Back	Close

Full Screen / Esc

Printer-friendly Version

Interactive Discussion

Abstract

In high-nutrient low-chlorophyll waters of the western Atlantic sector of the Southern Ocean, an intense phytoplankton bloom is observed annually north of South Georgia, most likely due to an enhanced supply of the limiting micronutrient iron. Shallow sediments and atmospheric dust deposition are believed to be the main iron sources. However, their relative importance is still unclear and in the South Georgia region have yet not been ascertained because iron measurements are very few. In this study, we use austral summer dissolved iron (dFe) data around South Georgia (January and February 2008) with a coupled regional hydrodynamic and biogeochemical model to investigate natural iron fertilization around the island. The biogeochemical component of the model includes an iron cycle, where sediments and dust deposition are the sources of iron to the ocean. The model captures the characteristic flow patterns around South Georgia, hence simulating a large phytoplankton bloom to the north, i.e., downstream, of the island. Modelled dFe concentrations agree well with observations (mean difference and root mean square errors of ~ 0.02 nM and ~ 0.81 nM) and form a large plume to the north of the island that extends eastwards for more than 800 km. In agreement with observations, highest dFe concentrations are located along the coast and decrease with distance from the island. Sensitivity tests indicate that most of the iron measured in the main bloom area originates from the coast and the very shallow shelf-sediments (depths < 20 m) while dust deposition plays a minor role, with almost no effects on surface chlorophyll a concentrations. Iron sources such as run-off not represented explicitly in the model, but that likely contribute to the iron plumes observed around South Georgia, are also discussed together with the potential effects their temporal variability may have on the system.

1 Introduction

The island of South Georgia is located in the western Atlantic sector of the Southern Ocean at the northeastern limit of the Scotia Sea, along the North Scotia Ridge (Figs. 1 and 2 for topographic features in the region), and lies between two of the main fronts of the easterly flowing Antarctic Circumpolar Current (ACC): the Polar Front (PF) and the Southern ACC Front (SACCF). The PF crosses the North Scotia Ridge at Shag Rocks Passage and then flows east remaining always due north of the island; the SACCF reaches South Georgia from the southwest, it flows along the southern shelf of the island and then veers anticyclonically towards the Georgia Basin before resuming its eastwards course (Orsi et al., 1995; Thorpe et al., 2002). Because of this large meander in the SACCF, waters downstream of South Georgia are transported to the northwest and north of the island. The ACC and its fronts control the physical and chemical properties of the waters surrounding South Georgia (i.e., Whitehouse et al., 1996; Korb and Whitehouse., 2004). In particular, the PF traces the boundary between the silicate poor waters observed to its north and the silicate rich waters to its south. Consequently, at the beginning of the growth season all macronutrients are at excess concentrations for phytoplankton growth: nitrates and silicates normally range 20–30 nM, whereas phosphates concentrations are close to 1.3–2 nM (CARS 2009; Ridgway et al., 2002).

Despite South Georgia's relatively small size ($\sim 3700\,\mathrm{km}^2$), satellite ocean colour imagery from the north and northwest of the island reveal a large ($\sim 145\,000\,\mathrm{km}^2$, Borrione and Schlitzer, 2013) and long-lived phytoplankton bloom with chlorophyll a (Chl a) concentrations often greater than $10\,\mathrm{mg\,m}^3$ (Korb et al., 2004) leading to one of strongest seasonal atmospheric-carbon uptake in the open Southern Ocean (Jones et al., 2012). These very high levels in pigment biomass concentrations are in sharp contrast with the surrounding high-nutrient low-chlorophyll (HNLC) waters, where, despite the presence of high macronutrient concentrations, phytoplankton blooms are observed only on few occasions (Fig. 1).

Title Page

Abstract | Introduction

Conclusions | References

Tables | Figures

◀◀ | ▶▶

◀ | ▶

Back | Close

Full Screen / Esc

Printer-friendly Version

Interactive Discussion

The environmental conditions behind South Georgia's very high primary productivity are still investigated; ongoing research has indicated that a continuous supply of iron from the island's shelf is most likely one of the most important drivers (Nielsdóttir et al., 2012). The currents flowing along and over the wide (30–100 km) continental shelf of the island could pick-up iron from shelf sediments and would then transport the iron-enriched waters towards the Georgia Basin, where intense blooms are regularly found (Nielsdottir et al., 2012; Korb et al., 2008; Borrione and Schlitzer, 2013). Clearly, sources of iron other than the South Georgia coastal region are possible. Among these there is atmospheric deposition of dust particles originating from the Patagonian Desert (Meskhidze et al., 2007; Johnson et al., 2010). Nevertheless, it is still impossible to ascertain from in situ data the magnitude and relative contribution of coastal processes and dust deposition on natural iron fertilization around the island because measurements of iron from the coast of the island are still very few (Holeton et al., 2005; Nielsdóttir et al., 2012) and direct estimates of dust-deposition are absent. In our current state of knowledge biogeochemical modelling remains the key tool, however to date such studies are absent for South Georgia, as they mostly considered the Southern Ocean as a whole (i.e., Tagliabue et al., 2009; Moore and Braucher, 2008).

In this study we investigated iron fertilization around South Georgia using a coupled model including the hydrodynamic regional model ROMS (i.e., Regional Oceanic Modelling System; Shchepetkin and McWilliams, 2005) and the biogeochemical model PISCES (i.e., Pelagic Integration Scheme for Carbon and Ecosystem Studies; Aumont and Bopp, 2006). In addition to the source of iron from dust deposition accounted for alone in previous models (i.e., Parekh et al., 2004; Aumont et al., 2003), PISCES also includes a sedimentary source of iron to the ocean. According to Moore and Braucher (2008) and Elrod et al. (2004), both iron sources must be present in ocean biogeochemical models including iron-limitation.

After introducing the modelling tools and observational datasets, we evaluate the model's performance in the South Georgia area and in particular the model's ability to simulate surface dissolved iron (dFe) concentrations. Finally, we present results from

sensitivity runs, performed to identify the main sources and distribution-pathways of dFe concentrations in the region. These results provide an opportunity to investigate natural iron fertilization around and downstream of South Georgia complementing the current lack of spatially-uniform in situ dFe measurements.

2   Model description

2.1   The hydrodynamic model ROMS

The hydrodynamic model used for this study is the version of ROMS (Shchepetkin and McWilliams, 2005) which makes use of the Adaptive Grid Refinement in Fortran (AGRIF) procedure, (i.e., ROMS_AGRIF; Debreu and Blayo, 2008; Penven et al., 2006).

ROMS_AGRIF is a three-dimensional, split-explicit, free-surface, primitive equation model. Vertical and horizontal coordinates are discretized in coastline and terrain-following curvilinear coordinates (i.e., sigma-layers) using high-order numerical methods. ROMS_AGRIF is based on the Boussinesq approximation and hydrostatic vertical momentum balance and solves the free surface primitive equations in an Earth-centred rotating environment. The model's code (version V1.1) and the pre- and post-processing routines (Penven et al., 2008) used in this study, together with the biogeochemical model PISCES described below, were obtained from the webpage of the Institut de Recherche pour le Développement (http://www.romsagrif.org/). To date, ROMS_AGRIF has been utilized for several oceanographic settings (i.e., Karakas et al., 2006; Penven et al., 2006), but never for a region of the Southern Ocean.

2.2   The biogeochemical model PISCES

PISCES (Aumont and Bopp, 2006) is a 24-compartment biogeochemical model. It simulates the biogeochemical cycles of oxygen, carbon and the cycle of the main micro-

and macronutrients controlling phytoplankton growth, i.e., iron, phosphate, nitrate, ammonia and silicate. The phytoplankton compartment comprises nanophytoplankton and diatoms; of the two, only the latter requires silicate for growth. Moreover, PISCES includes a grazer compartment (i.e., micro- and meso-zooplankton) as well as a non-

5　living detritus compartment, consisting of big and small organic particles. In all living compartments the total biomass in carbon is calculated explicitly and the Redfield C/N/P ratios are assumed constant and equal to 122/16/1. Additionally, for the phytoplankton compartment PISCES explicitly calculates values for chlorophyll (Chl), iron and, for diatoms only, silicate; consequently, the internal ratios for Fe/C, Chl/C, and

10　Si/C, which are allowed to vary, are always known. Conversely, for the zooplankton compartment these ratios are kept constant. The bacterial pool is not modelled explicitly.

The presence of an iron cycle (briefly described below and schematically represented in Fig. 3) is the key aspect of PISCES when performing biogeochemical mod-

15　elling in the iron-limited HNLC Southern Ocean.

In PISCES iron is supplied to the ocean in dissolved form from atmospheric dust-deposition and sediment mobilization. Aeolian deposition of iron to the ocean has been estimated from the climatological monthly maps of dust deposition modelled by Tegen and Fung (1995). Their annual estimates of dust deposition around South Georgia

20　(i.e., $1–5\,g\,m^{-2}\,yr^{-2}$) are comparable to those obtained with more recent modelling experiments (Mahowald et al., 2005; Ginoux et al., 2001). In the current configuration of PISCES, the iron content and its solubility in dust particles is constant and set to 3.5 %, and 2 % respectively. Similar percentages were used in previous biogeochemical models including iron (Moore and Braucher, 2008; Parekh et al., 2004). Once in the water

25　column, dust particles sink at $5\,m\,day^{-1}$ and undergo remineralisation until they reach the sea-floor and are lost to the sediments (Aumont and Bopp, 2006).

The flux of dFe from the sediments to the water column is calculated adapting the meta-model of Middelburg et al. (1996), here used to estimate the reductive mobilization of iron. The dFe flux depends on the maximum iron-flux at the sediment–water in-

terface (parameterized to $1\,\mu mol\,dFe\,m^{-2}\,day^{-1}$, which is close to $2\,\mu mol\,dFe\,m^{-2}\,day^{-1}$ used by Moore and Braucher, 2008) and depth. In the calculations depth is used as a proxy for how well the sediments are oxygenated.

DFe in free inorganic form (Fe′ in Fig. 3) can undergo complexation with one type of ligands (L′ in Fig. 3), which are present at uniform concentrations (i.e., 0.6 nM, see also Johnson et al., 1997) or scavenging on particles; the latter depends on the total load of organic particles and together with aggregation processes leads to the formation of particulate organic iron. Particulate organic iron is reintroduced into the dFe pool via remineralization, or it is lost to the sediments with sinking particles.

Previous simulations including the biogeochemical model PISCES have shown its ability to reproduce adequately global dFe and pigment biomass distributions proving it to be an appropriate tool for a variety of studies concerning ocean biogeochemistry, including those in the Southern Ocean (Aumont and Bopp, 2006; Slemons et al., 2009; Tagliabue et al., 2009).

2.3 Model configuration and simulations

In the present configuration, the coupled ROMS_AGRIF-PISCES model was implemented over the ocean domain depicted in Fig. 1, defined between (60–20° W) and (60–40° S) with a resolution of approximately 11 km. The size of the domain was chosen in order to maintain sufficient distance between South Georgia and the domain-boundaries, thus limiting the effects of the four open-boundary conditions on the solutions (see also Young et al., 2011). At the average latitude and longitude of the model-domain, the Rossby radius is ∼ 15 km (Chelton et al., 1998), indicating that the current resolution is eddy permitting. Along the vertical dimension we used 32 sigma-coordinate layers stretched to increase vertical resolution near the surface.

ETOPO2 (Smith and Sandwell, 1997) was used to construct the model bathymetry. To prevent horizontal pressure gradient errors, the ETOPO2 topography was smoothed. In our configuration, the variable that controls the maximum value of the r-parameter

measuring the slope of the sigma-layers is set to 0.25 (Beckmann and Haidvogel, 1993). Water temperature, salinity, sea level and velocity fields used at the boundaries and for the model's initial conditions derive from the Simple Ocean Data Assimilation reanalysis (SODA, Carton and Giese, 2008). The SODA physical ocean properties
5   were retrieved from the web (http://iridl.ldeo.columbia.edu/) and elaborated with the ROMSTOOLS pre-processing toolbox (Penven et al., 2008) to construct the climatology used in the simulations.

The model is forced with fresh water and heat fluxes from the Comprehensive Ocean–Atmosphere Data Set (COADS05, Da Silva et al., 1994), while the surface
10 wind stress climatology for the 2000–2007 time-period derives from QuikSCAT measurements (Quick scatterometer, http://www.ifremer.fr/opendap/cerdap1/cersat/wind/l4/quikscat/daily/). A climatology of sea surface temperatures from Pathfinder satellite observations (Casey and Cornillon, 1999) was utilized to restore modelled surface temperatures.

15 PISCES boundary and initial conditions for dFe, macronutrients (i.e., nitrate, phosphate, silicate) and oxygen were derived from the World Ocean Atlas 2005 climatological datasets (Conkright et al., 2002) included in the ROMSTOOLS pre-processing toolbox, while the boundary and initial conditions for Chl a, phytoplankton and zooplankton biomass were obtained from existing ORCA2 model simulations (Aumont and
20 Bopp, 2006), and successively adapted to the current domain size, grid structure and resolution.

Model spin-up was carried out for 20 yr, until quasi-equilibrium was reached, and then ran for 10 more yr. In addition to the reference simulation, hereafter called SED-DUST, in which boundary conditions, surface forcings and iron sources are equivalent
25 to those described above, we performed sensitivity runs in which we modified the iron sources present in the last three modelling years. All sensitivity runs are listed in Table 1. In two sensitivity runs either sedimentary or aeolian sources of iron were removed from the system (simulations are named NOSED_DUST and SED_NODUST, respectively). In each of the other sensitivity runs, atmospheric sources of iron were kept

identical to those utilized in the SEDDUST scenario, whereas the reductive mobiliza-
tion of iron was limited to sediments present at selected 5 m-thick ocean depth inter-
vals. Six simulations resolved the top 0–30 m surface layer, while in two additional runs
reductive mobilization of iron was limited to the sediments present at the 50–55 m and
100–105 m ocean depths intervals only. When compared to the reference SEDDUST
scenario, these sensitivity simulations provide information on the relative importance
of dust and sedimentary sources, but also provide an indication of the depth of the
sedimentary sources contributing most of the dFe observed at the surface. Results are
presented in Sect. 4.5 below.

All model results shown in the following are obtained from the averages of January
and February of the last modelling year, because for these months in situ surface dFe
data are available for the validation of our results (Nielsdóttir et al., 2012).

3 Observational dataset

3.1 Ocean colour measurements

Freely available Aqua MODIS (Moderate Resolution Imaging Spectroradiometer) Stan-
dard Mapped Images – Level 3 products, for the ocean-colour monthly composites of
January and February from the 2006–2011 time-period, processed by the Goddard
Space Flight Center and projected on a regular spatial grid of 9 km, were retrieved
from the Distributed Active Archive Center (http://oceancolor.gsfc.nasa.gov/). The full
dataset was used to construct the climatology depicted in Fig. 1, while the averages
obtained from the monthly composites of January and February 2008, corresponding
to the sampling-period of in situ surface dFe concentrations (Nielsdóttir et al., 2012,
see below), and the averages obtained from the monthly composites of January and
February 2011 were used for comparisons with model outputs (Fig. 6). Ocean colour
estimates depicted in Fig. 6a and b were interpolated onto the model's coarser grid
resolution (∼ 11 km).

3.2 Surface water circulation

Surface circulation patterns in the South Georgia area (region outlined with a rectangle in Fig. 1) were estimated from Aviso satellite altimetry (http://www.aviso.oceanobs.com/duacs/). The Aviso altimeter product is based on multiple altimeter missions (Jason-1 and 2, T/P, Envisat, GFO, ERS-1 and 2 and Geosat) and provides a consistent and homogeneous dataset. Weekly delayed-time values for the zonal and meridional components of surface current velocity computed from absolute topography, re-sampled on a regular 0.25° grid, were extracted for the months of January and February of 2008 for comparisons with modelled surface (0–30 m) velocities (in Fig. 4), but also for January and February of 2011 (Fig. 6b).

3.3 Macronutrients

Surface (0–30 m) concentrations of nitrate, phosphate and silicate, distributed by the CSIRO Atlas of Regional Seas (CARS; http://www.marine.csiro.au/~dunn/cars2009/; Ridgway et al., 2002) and available at a 0.5° grid resolution, were retrieved and then averaged for the area centred around the main South Georgia bloom region (45–32° W; 56–50° S in Fig. 7a). The annual cycles of the three macronutrients were compared with those obtained with the model during the last modelling year (Fig. 5).

3.4 In situ surface dFe measurements

Underway surface dFe measurements around South Georgia were obtained during an oceanographic cruise to the Scotia Sea aboard the *RRS James Clark Ross*, as part of the British Antarctic Survey Discovery 2010 FOODWEBS programme. DFe concentrations used in this study are from the period between 23 January and 10 February 2008. All dFe underway samples were treated and determined as described in detail by Nielsdóttir et al. (2012). Sample locations and measured values are shown in Fig. 2c of Nielsdóttir et al. (2012) and in Figs. 7a and 8a of the present manuscript.

Title Page

Abstract | Introduction

Conclusions | References

Tables | Figures

|◄ | ►|

◄ | ►

Back | Close

Full Screen / Esc

Printer-friendly Version

Interactive Discussion

4   Results

In the following, we first assess the ability of the model to reproduce environmental conditions around South Georgia by comparing physical and biogeochemical conditions obtained from model simulations with available observational data. For consistency with the time period of the available surface dFe concentration dataset (Niels-dóttir et al., 2012), surface circulation and ocean colour pertain to January–February of 2008, while model results are from surface (0–30 m) averages of January–February of the last modelling year. To assess the sensitivity of the results to the chosen period, we also considered previous years but found comparable results in all cases. Similar results are obtained because the model was in a quasi-equilibrium state but also because boundary conditions and forcing fields derive from climatologies that are repeated cyclically in each year of the simulations. For the same reason, modelling results shown in the following cannot reproduce the details of any observational year. Second, we use model results to describe the potential distribution of surface dFe concentrations around South Georgia, as well as its principal sources.

4.1   Circulation patterns around South Georgia

Surface circulation patterns estimated from Aviso satellite altimetry during January and February of 2008 and those obtained from model simulations are compared in Fig. 4 to evaluate the ability of the model to reproduce the main features of circulation around South Georgia. Satellite altimetry (Fig. 4a) indicates that the ACC, the principal current around South Georgia, enters the South Georgia area from the southwest and crosses the North Scotia Ridge at three locations: close to Shag Rocks Passage ($\sim 48°$ W, $53°$ S), at Black Rock Passage, which is located between Shag Rocks and South Georgia ($\sim 40°$ W, $54°$ S), and to the east of the island following closely the 2000 m bathymetry contour (Fig. 4). The latter branch of the ACC turns west along the northern flank of the island flowing towards the Georgia Basin. On its way the current is joined by the flow through Black Rock Passage at first and subsequently also by part

Title Page

Abstract | Introduction

Conclusions | References

Tables | Figures

◀ | ▶

◀ | ▶

Back | Close

Full Screen / Esc

Printer-friendly Version

Interactive Discussion

of the flow that crosses the North Scotia Ridge through Shag Rocks Passage. Over the Georgia Basin, the circulation is cyclonic and characterized by intense currents along the margins of the basin (~ 20–$25\,\mathrm{cm\,s^{-1}}$), and by weaker currents over the central portion of the basin (often below 10–$15\,\mathrm{cm\,s^{-1}}$). Once the flow exits the Georgia Basin it continues east along a convoluted route close to NEGR and the Islas Orcadas Rise (refer to Fig. 2 for topographic features in the region).

For the purposes of this study, which aims at understanding sources but also potential transport pathways of iron from and then around South Georgia, particularly important circulation features are (i) the current that flows westwards along the northern shelf of the island towards the Georgia Basin, believed to transport iron-enriched waters from the shelf region towards the bloom area (Nielsdóttir et al., 2012); (ii) the intense cyclonic circulation along the borders of the Georgia Basin, which confine South Georgia blooms to the basin (see Borrione and Schlitzer, 2013) and (iii) the flow across Black Rock Passage which delimits the southwestern border of South Georgia blooms separating them from the waters adjacent to Shag Rocks (see Venables et al., 2012). The level of realism reached by the simulated surface circulation during January and February (Fig. 4b) will be assessed considering these specific currents. Smaller scale features, like eddies, filaments or meanders in the flow, are not considered in the comparison between altimetry and modelling results because they reflect the natural variability of the system, and can be very different according to the years considered.

During January and February of the last model year (Fig. 4b), surface circulation patterns around the island are strongly steered by bottom topography, and reflect in many ways circulation patterns described from satellite altimetry (Fig. 4a). In fact, the model reproduces the current that after flowing along the southeastern and then the northeastern shelf of the island splits into a branch that flows northeast of the island, along the southern flank of the NEGR, or veers west travelling along the northern shelf of the island towards the Georgia Basin. Moreover, the model reproduces the northwards current flowing across Shag Rock Passage or across the Black Rock Passage.

Along the margins of the Georgia Basin the current is relatively intense (20–40 cm s^{-1}) whereas over the central portion of the basin the current is generally weaker (10–15 cm s^{-1}), except for a fast rotating anticyclonic eddy that is formed to the south west of the basin (40° W, 53° S). This eddy is not present in the Aviso observations for January–February of 2008.

Modelled current intensities reproduce the general spatial variability observed in satellite altimetry. For example, in both the modelled and satellite-based circulation fields, surface currents are stronger along the margins than over the central part of the basin; overall, however, the model tends to overestimate absolute circulation velocities.

4.2 Macronutrient concentrations

Macronutrient surface (0–30 m) concentrations averaged over the domain centred around the main South Georgia bloom area, defined between 45–32° W and 56–50° S (shown in Fig. 7a) follow a clear annual cycle both in the CARS2009 and modelled data (Fig. 5). For both datasets and all macronutrient variables, maximum values occur between winter and early spring, while minimum values are recorded in early austral summer; furthermore, in all cases surface macronutrient concentrations averaged over the chosen domain are above concentrations that are limiting for phytoplankton growth. In the following, maximum and minimum values are reported with their corresponding standard deviation (SD) and one standard error interval (SE).

In the two datasets, the timing of maximum and minimum values in the annual cycles of silicate coincide (Fig. 5a). During September surface silicate concentrations reach their annual maximum value and rise to $\sim 25\,\mu$M in the CARS2009 dataset (SD $\sim 8.9\,\mu$M and SE $\sim 0.47\,\mu$M) and in the model (SD $\sim 8.63\,\mu$M and SE $\sim 0.12\,\mu$M). In February, however, when silicate surface concentrations are at their minimum, concentrations are significantly different: in the CARS2009 dataset concentrations are close to $7.16 \pm 5\,\mu$M (SE $= 0.34\,\mu$M) and correspond to approximately 28 % of the maximum value recorded in September; conversely, in the model silicate concentrations during February are almost twice those of the CARS2009 dataset; modelled silicate concen-

trations are close to $15.45 \pm 7.7\,\mu M$ (SE $\sim 0.11\,\mu M$) and correspond to 62 % of the maximum value recorded in September. Therefore, in the model there is a significantly weaker winter-summer reduction of silicate concentrations than in the CARS2009 observations, possibly due to the model's tendency to underestimate total Chl *a* (see below) or to the model's range of admitted Si/C ratios.

As shown in Fig. 5b, the model matches the timing of maximum and minimimum nitrate concentrations observed in the CARS2009 dataset (i.e., September and February in both datasets). However, compared to the CARS2009 surface nitrate concentrations, which range between $\sim 20.44 \pm 1.65\,\mu M$ in February (SE $\sim 0.09\,\mu M$) and $30.1 \pm 2.5\,\mu M$ in September (SE $\sim 0.13\,\mu M$), the annual cycle of modelled surface nitrate concentrations averaged over the South Georgia domain are approximately $4\,\mu M$ lower than observations: in the model, nitrate concentrations range between $17.5 \pm 2.22\,\mu M$ in February (SE = $0.03\,\mu M$ L) and $24 \pm 1.66\,\mu M$ in September (SE = $0.03\,\mu M$). Despite the negative bias in modelled concentrations, like in the observations modelled minimum values during summer derive from a ~ 30 % reduction of the maximum winter values.

The annual cycles of CARS2009 and modelled phosphate concentrations averaged over the South Georgia area are indicated in Fig. 5c. Observational and modelled phosphate concentrations range between very similar values: minimum values are respectively $1.37 \pm 0.13\,\mu M$ and $1.36 \pm 0.12\,\mu M$, while maximum concentrations are respectively $1.88 \pm 0.08\,\mu M$ and $1.8 \pm 0.01\,\mu M$. In the two datasets however, the months of minimum and maximum values differ: in the CARS2009 dataset, they occur respectively in February and October, while in the model minimum and maximum values are observed respectively in March and September.

4.3 Surface Chl *a* concentrations

During January–February of 2008, MODIS satellite estimates of surface Chl *a* concentrations (Fig. 6a) reveal the presence of a large and intense phytoplankton bloom over the southern and northwestern shelf of South Georgia, and to the northwest and north of the island (Chl $a > 2\,\mathrm{mg\,m^{-3}}$). The bloom reflects the geometry of the typical bloom

Title Page

Abstract | Introduction

Conclusions | References

Tables | Figures

◄◄ | ►►

◄ | ►

Back | Close

Full Screen / Esc

Printer-friendly Version

Interactive Discussion

area described by Borrione and Schlitzer (2013). Outside all borders of the Georgia Basin and due east of the island Chl a values fall close to or below $0.5\,\mathrm{mg\,m^{-3}}$ (HNLC waters). In this specific period of observations, exceptions to the HNLC waters observed outside the main bloom area are the patches around (42° W, 55° S), (43–49° W, 48° S) and (24° W, 53° S) where Chl a concentrations are above $0.75\,\mathrm{mg\,m^{-3}}$. The latter Chl a rich patch, which is more than 700 km east of the NEGR, is much larger in size than the previous patches, and appears to be connected to the main bloom area by a narrow filament with Chl a concentrations $\sim 1\,\mathrm{mg\,m^{-3}}$.

Arrows in Fig. 6a represent contemporaneous surface circulation patterns from Aviso satellite altimetry (see also Sect. 4.1 and Fig. 4a). The joint analysis of the two datasets shows that the location and shape of the South Georgia bloom is strongly related to local circulation, which seems to also generate the narrow tongue of Chl a rich waters connecting the main bloom area to the Chl a rich patch observed around (24° W, 53° S). Moreover, over the shelf of the island variability in flow intensity is reflected in the distribution of Chl a concentrations. In fact, over the western and southern shelf of the island, where Chl a concentrations are highest, surface circulation is very weak ($< 5\,\mathrm{cm\,s^{-1}}$), while over the northeastern portion of the shelf region, where Chl a concentrations are low ($< 0.2\,\mathrm{mg\,m^{-3}}$) surface currents flowing parallel to the shelf-break are above 10–$15\,\mathrm{cm\,s^{-1}}$.

During January–February of 2011 (Fig. 6b), Chl a concentrations were mostly below $1.5\,\mathrm{mg\,m^{-3}}$ and provide an example of a weaker South Georgia phytoplankton bloom. Nevertheless, patterns in Chl a concentrations (i.e., location of bloom and non-bloom waters) and surface circulation around the island have many similarities with the patterns described for January–February of 2008 (Fig. 6a).

Surface Chl a concentrations obtained from the average of January and February from the last modelling year (SEDDUST scenario) are shown in colour in Fig. 6c. In the same figure, black arrows depict contemporaneous modelled surface circulation patterns. Comparison between modelled surface Chl a concentrations and surface velocities (Fig. 6c) with satellite observations (Fig. 6a) shows the ability of the model to

capture the main features of primary productivity in the South Georgia region: in the modelling and observational datasets highest productivity levels are observed over the Georgia Basin and the shelf of the island, where Chl a concentrations are one order of magnitude higher than in the surrounding waters. Moreover, in both datasets the phytoplankton bloom extends in the west-east direction between the area north of Shag Rocks and the NEGR, and it extends in the north-south direction between the 50° S parallel and the southern shelf-break of the island. In agreement with satellite ocean colour imagery, ROMS_AGRIF-PISCES reproduces the long ($\sim$ 800 km) Chl a rich plume extending eastwards of the NEGR, but also a region of higher productivity along the Falkland Escarpment, to the northwest of the South Georgia phytoplankton bloom. Although the current model configuration does not allow for a reproduction of a specific year of observations, it must be noted that overall the model can capture adequately the relative magnitude of Chl a concentrations between bloom and non bloom waters. However the model tends to under-estimate absolute Chl a concentrations as shown by comparing model results with Chl a concentrations observed in 2008 (Fig. 6a), but also those observed during the less productive austral summer of 2011 (Fig. 6b). In the model in fact, highest Chl a concentrations are mostly between 0.7–1.5 mg m^{-3} in the main bloom area, while in the relatively wide plume extending downstream of the NEGR, Chl a concentrations never rise above 0.3 mg m^{-3}.

Similarly to our description of MODIS Chl a concentrations and Aviso altimetry (Fig. 6a and b), also in the modelled fields (Fig. 6c) there is a clear correspondence between productivity patterns and local circulation. In fact, in the simulations the South Georgia phytoplankton bloom is confined at all sides by bands of rapidly flowing currents (20–40 cm s^{-1}), while the two Chl a rich plumes observed along the Falkland escarpment and downstream of the NEGR correspond to regions of very high flow velocities (30–80 cm s^{-1}), which most likely are responsible for the position, shape and extension of the two Chl a rich plumes. Over the southern portion of the Georgia Basin (40° W, 53° S), amidst waters with high Chl a concentrations, an anticyclonic eddy encircles waters with very low Chl a concentrations ($\sim$ 0.1 mg m^{-3}). Analysis of circulation

and Chl *a* concentration fields from previous modelled months, indicates that the anticyclonic eddy detaches from a meander extending southwards from the Chl *a* poor waters to the north of the Georgia Basin. A similar meander is observed in satellite imagery of January 2004 (Borrione and Schlitzer, 2013).

4.4 Surface dFe concentrations

Surface ($\sim$ 3 m) underway dFe concentrations (in Fig. 7a, see also Nielsdóttir et al., 2012) were measured between January and February 2008 in the area south of South Georgia ($\sim$ 41° W, 55° S), along a transect across the Georgia Basin, and over the northern shelf of the island. Surface dFe concentrations were highest over the shelf of the island, ranging between 2.5 and 6.9 nM and then decreased to concentrations of approximately 1 nM close to the 2000 m bathymetry contour. Over the Georgia Basin, concentrations were variable and ranged between values close to the instrumental detection limit (0.027 ± 0.018 nM) and high concentrations (i.e., 2 nM at 38° W, 52.5° S). South of South Georgia, i.e., upstream of the island, dFe concentrations were very low (≤ 0.1 nM) at all sampled locations.

DFe concentrations measured in the locations marked in Fig. 7a, are also depicted in Fig. 7b following their sampling progression for a more detailed comparison with model results. Modelled surface (0–30 m) dFe concentrations from January and February of the last model year (SEDDUST scenario; Fig. 7b) were interpolated onto the same sampling locations in order to maintain in both datasets the correspondence of dFe concentrations with local topography (i.e., distance from the island or ocean depth). As in the current model configuration, boundary conditions and forcing fields derive from a cyclical climatology, and hence model results cannot be representative of any specific observational year, we will compare the relative variability of dFe concentrations in the region, and not absolute dFe concentrations. In both datasets dFe concentrations increase progressively from the area upstream of South Georgia (on average, dFe < 0.1 nM), to the Georgia Basin (on average, dFe concentrations between 0.5 nM and 2 nM) and finally to the area over the shelf of the island, where concentrations are

maximum in both datasets (on average, dFe concentrations between 1.5 nM and 6 nM). Differences in the absolute measured and sampled dFe concentrations, as for example over the southern part of the Georgia Basin (indicated as South GB in Fig. 7), depend on differences between surface circulation patterns in the two datasets: comparing Fig. 6c with Fig. 6a, it can be seen that around (40° W, 53° S) model results indicate the presence of an anticyclonic eddy which is not present in the surface circulation patterns obtained from satellite altimetry for 2008.

On average, the difference between modelled and measured dFe concentrations in the locations marked in Fig. 7a is ~ 0.02 nM, with root mean square (RMS) close to 0.81 nM. Similar values were also obtained when dFe concentrations were extracted from the austral summers of the two previous modelling years (data not shown): in the previous years the calculated mean difference is ~ 0.01 nM and the RMS is close to 1 nM. These low values demonstrate that in the present configuration, the model can reproduce adequately the main features of the distribution of dFe concentration in the region; moreover, similarly to the in situ dataset, modelled dFe concentrations are at their minimum values to the south, i.e., upstream, of the island and reach their maximum concentrations along the coastal area.

Clearly, modelling results can provide a picture at uniform spatial resolution (~ 11 km) of surface dFe concentrations also outside the locations indicated in Fig. 7a. During January and February of the last modelling year, surface dFe concentrations (Fig. 8a) are < 0.1 nM in most of the South Georgia domain, except for a large area over the shelf and to the north and northeast of the island and over a narrow area along the Falkland Escarpment, located to the northwest of South Georgia.

Over the shelf of South Georgia dFe concentrations are overall > 2 nM, with highest values along the coast (2–8 nM). An iron rich plume (~ 0.5 nM) originates from the northwestern corner of the shelf and extends westwards along the northern flank of Shag Rocks; a second dFe plume originates from the northeastern shelf of the island and extends northeastwards along the flanks of the NEGR. The latter plume continues further east along the Islas Orcadas Rise for approximately 800 km, until dFe concen-

Sedimentary and atmospheric sources of iron around South Georgia

I. Borrione et al.

Title Page

Abstract	Introduction
Conclusions	References
Tables	Figures

◀ | ▶

◀ | ▶

Back | Close

Full Screen / Esc

Printer-friendly Version

Interactive Discussion

trations reach background values (< 0.1 nM). Both plumes are clearly dependant on the direction of flow (black arrows), which here moves away from the island, and its high velocities (~ 20–$50 \, \mathrm{cm \, s^{-1}}$). Conversely, to the south and east of the island, surface dFe concentrations decrease rapidly to background concentrations (< 0.1 nM), remaining
5 high only along a narrow band over the southern shelf of the island; such limited extension is due to the local currents which here move northwards pushing surface waters towards the coast, and then in the easterly direction.

The scale length (Johnson et al., 1997) provides a way to quantify the decrease of iron with distance; its value accounts for all processes acting to increase or decrease
10 surface dFe concentrations, without discriminating between them. The scale length of dFe transport is defined as the distance over which an initial reference concentration (RC) drops to $1/e \cdot$ RC. For our calculations, as reference we use the average dFe concentration along the coast of the island (i.e., 3.68 nM). In Fig. 8b (detail of Fig. 8a) the position of dFe concentrations equal to $1/e \cdot 3.68$ nM (i.e., 1.35 nM) is traced with
15 a thick contour line. The dFe scale length corresponds to the distance between the coast of the island and the 1.35 nM contour line.

In the chosen time-period, modelling results clearly show that the scale length of dFe concentrations is a dynamic property, and that it can vary of a factor of ~ 5 depending on the direction and intensity of local circulation. In fact, to the south of the island, where
20 the flow pushes surface waters towards the coast and then in the easterly direction, the scale length is at its minimum values (~ 20 km), while to northwest of South Georgia, where local circulation is directed away from the island towards the Georgia Basin, the scale length reaches its maximum values (~ 110 km).

4.5 Iron sources around South Georgia

4.5.1 Atmospheric sources of iron

25

Scale lengths ranging between 20 and 110 km have clearly shown that South Georgia is the core of the dFe plume observed in the region. However, as South Georgia is

located along the main trajectory of dust plumes originating from the Patagonian desert (Mahowald et al., 2005; Ginoux et al., 2001; Johnson et al., 2010) dust deposition may also be a source of iron to the surface waters around the island.

The importance of dust-derived dFe to the surface layer was evaluated by comparing results from the reference SEDDUST scenario with the SED_NODUST sensitivity run. Surface dFe concentrations obtained with the two simulations and extracted along the virtual transect line traced in Fig. 8a are marked respectively with a solid and dashed red line in Fig. 8c. The transect line was chosen in order to consider regions of the South Georgia domain which are closer or farther from the island or the Patagonian desert, and hence likely differ on the relative importance of sedimentary or dust sources of iron. Results depicted in Fig. 8c indicate that along the transect east of ∼ 48° W, the contribution of dFe from dust deposition is approximately 0.01 nM, hence negligible when compared to surface concentrations from the SEDDUST run, especially over the Georgia Basin. Conversely, in the area around (49° W, 48° S), at the northwestern corner of the South Georgia domain, atmospheric deposition is the principal source of dFe to the region; in fact, in the SEDDUST simulation, dFe concentrations are ∼ 0.1 nM, but drop to values close to zero when the dust source of iron is removed.

The greater importance of sedimentary versus atmospheric sources of iron in the domain centred around the main bloom area (Fig. 7a) is confirmed by averaged surface dFe and Chl a concentrations obtained either with the SEDDUST or SED_NODUST simulation. As shown in Table 1, average values from the SED_NODUST simulation are only slightly lower than those obtained with the SEDDUST run. Moreover the integrated dust deposition of dFe over the same domain (∼ 2200 km away from South America) is ∼ $6.27 \times 10^9 \, \mu\mathrm{M\,day^{-1}}$ while the flux of sedimentary iron released into the water column from all sediments shallower than 100 m is $1.35 \times 10^{11} \, \mu\mathrm{M\,day^{-1}}$. Nevertheless, it must be remarked that although the flux estimates presented above are useful for an estimate of the relative importance of the two main iron sources around South Georgia, their absolute values must be considered with care because model results rely on our current knowledge (and uncertainties) of the iron cycle, and may

largely depend on the chosen model parameters (i.e., content and solubility of iron in dust, or maximum dFe flux from the sediments, in Sect. 2.2).

4.5.2 Sedimentary sources of iron

Results presented in the previous section have indicated that in the model, sediments around South Georgia release almost all of the iron observed around and then downstream of the island. Therefore sensitivity runs were used to estimate the depth of the most significant sedimentary sources. For this purpose, in each sensitivity run sediments from a selected depth range only could act as sources of iron, while at all other depths the iron flux was set to $0\,\mu M\,m^{-2}\,day^{-1}$ (see Sect. 2.3). Surface dFe and Chl a concentrations obtained from the reference SEDDUST simulation and each sensitivity run and then averaged over the domain centred around the main bloom area (Fig. 7a) are compared in Table 1 and depicted in Fig. 9.

Results suggest that the island's coast and very shallow sediments (i.e., depths $\leq 5\,m$) account for most of the surface dFe and Chl a concentrations simulated with the SEDDUST scenario, followed in importance by sedimentary sources from the 5–20 m depth interval. Conversely, when the release of dFe occurs at greater depths only, the model generates a weak and localized surface dFe and Chl a plume (not shown), reflected in dFe and Chl a values that become progressively similar to those obtained with the NOSED_DUST simulation (Table 1). Moreover, surface dFe and Chl a concentrations obtained with the SEDDUST_100–105 m simulation (Fig. 9f and l) are almost identical to those obtained with the NOSED_DUST simulation (Fig. 9b and h). The similarity of results, is further confirmed by RMS and mean differences calculated between the two runs (last row of Table 1).

Although these results are very useful for an estimate of the relative importance of sedimentary sources of iron at different depths, it must be stressed that because in the present model configuration there is no effect of tidal mixing, and the chosen resolution does not allow the representation of vertical mixing generated at the meso and sub-

Title Page

Abstract   Introduction

Conclusions   References

Tables   Figures

◄   ►

◄   ►

Back   Close

Full Screen / Esc

Printer-friendly Version

Interactive Discussion

mesoscale, the contribution from the deeper layers could be largely underestimated (Blain et al., 2008).

5 Discussion

5.1 The South Georgia island mass effect

The work presented here derives from the first regional biogeochemical modelling study that investigates natural iron fertilization and its effects on Chl *a* concentrations around South Georgia.

Results obtained with ROMS_AGRIF-PISCES show that enhanced Chl *a* concentrations are only found downstream of South Georgia, i.e., to the north and then northeast of the island, suggesting that the South Georgia island mass effect, and not processes acting upstream of the island, stimulate the observed blooms. A similar conclusion was reported by Korb et al. (2004) who investigated the spatial variability of phytoplankton blooms with in situ and satellite-based observations. In the model, South Georgia phytoplankton blooms extend in the easterly direction for more than 800 km following the direction of the main flow and decrease in magnitude with distance from the island. Such long ranges are in agreement with previous satellite-based studies, and in particular with those of Korb et al. (2004) who observed that the South Georgia bloom can extend till the 0° meridian, for distances > 2700 km aligned to the main path of the Polar Front (see also Venables et al., 2012). Moreover modelling results, which we have shown to be able to capture the main features of dFe distribution revealed by available measurements, but also to reproduce relatively well absolute dFe concentrations (Figs. 7 and 8; root mean square 0.81 nM), can provide a comprehensive view of surface dFe concentrations in the region during the productive season, hence complementing the current lack of large scale and spatially-uniform in situ measurements.

As one could hypothesize observing surface Chl *a* concentration patterns, the modelled dFe plume extends over a large area to the north and then northeast of the island

Full Screen / Esc

Printer-friendly Version

Interactive Discussion

following local circulation. As previously measured around South Georgia (Nielsdóttir et al., 2012), but also in other regions of the Southern Ocean (e.g., Ardelan et al., 2010; Bucciarelli et al., 2001; Planquette et al., 2007) the model indicates highest dFe concentrations in near-shore waters (> 5 nM), decreasing with distance from the island. Our model results clearly show that the South Georgia island mass effect can reach regions located far away from the island (> 1000 km), where dFe concentrations may still be above background concentrations. A comparable long-range influence of coastal regions has been previously suggested in other open-ocean regions of the World's Ocean, including the Southern Ocean (Elrod et al., 2004; Lam et al., 2006; de Jong et al., 2012; Moore and Braucher, 2008).

DFe scale length values, calculated from our model results as the distances over which an initial reference concentration drops to $1/e$ of its initial value (Johnson et al., 1997), vary between 20 km and 110 km. These values include the wide range of scale lengths obtained from in situ dFe observations in the open ocean and near-shore regions of the Southern Ocean. Smallest values were obtained by Ardelan et al. (2010) around the Antarctic Peninsula, and by Planquette et al. (2007) around the Crozet Islands (∼ 25 km in both studies); larger scale lengths were calculated around South Georgia by Nielsdóttir et al. (2012) and in the vicinity of the Kerguelen Islands by Bucciarelli et al. (2001) (scale lengths respectively 102 km and 151 km). As shown in our model results around South Georgia (Fig. 8a) and by Ardelan et al. (2010) and Planquette et al. (2007) from in situ estimates, dFe scale lengths are variable and dependant on the direction and speed of local circulation. Clearly, it is important to keep in mind that scale length values do not depend on surface circulation only, but can be influenced by all processes that decrease or increase dFe concentrations between the source region and the points where scale lengths are measured (i.e., dilution, biological uptake; Nielsdóttir et al., 2012). Nevertheless, scale length calculations alone cannot discriminate between them.

5.2 Atmospheric and sedimentary sources of iron

In PISCES, dFe is supplied to the ocean from atmospheric dust-deposition and sediment mobilization (Fig. 3; Aumont and Bopp, 2006). Compared to the reference SEDDUST scenario, model results obtained removing atmospheric sources of iron (SED_NODUST simulation), show that there is a very small reduction ($< 1\%$) in surface iron concentrations over the main phytoplankton bloom area (Fig. 8c), reflected in a negligible change in surface Chl a concentrations. To the best of our knowledge, in situ measurements of dust-derived iron deposition around South Georgia are presently not available for a comparison with our results. However, similar results were obtained by Meskhidze et al. (2007): combining model-based fluxes of mineral dust deposition and satellite-based surface Chl a concentrations between March 2000 and January 2004, they observed that the sole deposition of dust from the Patagonian desert, considered the major source of dust deposited to the Atlantic Ocean (Johnson et al., 2010), does not provide the major input of iron to the South Georgia region.

The limited effect of dust-deposition on the iron budget and hence also on phytoplankton growth downstream of South Georgia suggested by our study and by Meskhidze et al. (2007) mostly likely resides on the fact that local circulation provides a continuous supply of sedimentary iron that can maintain high dFe concentrations throughout the productive season. In these conditions, any additional input of iron, unless particularly conspicuous, will have negligible effects on existing dFe concentrations. Conversely, outside the area influenced by any sedimentary input of iron from the island, surface background dFe concentrations are very low (< 0.1 nM) and any additional input of iron, including from dust deposition, can modify initial concentrations and stimulate phytoplankton growth. Similar conditions may explain the isolated patches of Chl a rich waters observed outside the main South Georgia bloom area (Fig. 6a). The importance of aeolian deposition of iron in regions that are land-remote and upstream sedimentary sources is in agreement with previous observations or modelling results for larger scale or global studies (Tagliabue et al., 2009; Moore and Braucher, 2008).

However, as reviewed by Mahowald et al. (2005) there are still many uncertainties in the current knowledge of the life cycle of dust particles, from their release into the atmosphere to their deposition on the ocean's surface, as well as on their interaction with the biological compartment (i.e., bacterial, phytoplankton or grazers activity; Baker et al., 2010).

As described in Sect. 4.4 (Figs. 7b and 8a), model results are able to capture the main features of dFe concentrations around the island, and suggest that the very shallow sediments provide most of the iron observed around and downstream of the island. Clearly, the absence of tidal forcing as well as the current coarse model resolution and smoothed topography will likely lead to an underestimation of all the fine scale mechanisms that can dilute the highly enriched coastal waters and control the spatial variability of biogeochemical properties around the island (i.e., continental shelf waves, cross-shelf or vertical mixing; Young et al., 2011). The absence of these processes may also explain the relatively homogeneous distribution of dFe concentrations around most of the island (Fig. 8a), reflected in a similar distribution of Chl *a* concentrations (Fig. 6c).

With the current model configuration we cannot discriminate between all potential physical and chemical processes introducing iron around the island. However, considering the characteristic topography, landscape and circulation around South Georgia, we expect the concomitant effect of the processes schematically represented in Fig. 10. We can distinguish two major categories: processes acting on land or along the coast (i.e., precipitation and run-off) responsible for the input of iron present or deposited on land, and processes acting in the ocean, due to physical, biological or chemical processes occurring in the water-column or at the sediment–water interface.

South Georgia is a mountainous and largely barren island, with an irregular coastline and rugged topography. Most of the island's surface is recurrently or permanently covered by snow and ice; many glaciers terminate at the coast or calve directly into the sea (Gordon et al., 2008). During austral summer, rain, melting snow and glaciers most likely have a double effect on iron input to the ocean: melt-water not only can

carry dust particles accumulated during winter, but, together with rain, it can feed local creeks, which hence have a stronger erosion effect on soil. All around the island, fine-sized particles and glacial-flour generate extensive plumes that are clearly visible in Landsat satellite images of South Georgia (see Fig. 3 in Young et al., 2011). Indeed,

5   because many glaciers terminate at the coast or calve into the sea, glacier-scoured debris and glacier calving can determine an additional input of trapped soil particles and/or dust to the ocean (i.e., Raiswell et al., 2008).

In PISCES the sedimentary sources of iron are simulated considering reductive mobilization (Aumont and Bopp, 2006), which has been recognized as a significant source

10 of dFe to the oceans; recent studies (i.e., de Jong et al., 2012; Klunder et al., 2011) suggest that the increase in dFe concentrations observed in measurements closer to the sea-floor most likely derive from reductive mobilization of iron. In particular, below very productive surface waters as those observed around South Georgia, the bacterial oxidation of deposited organic matter accentuates reductive conditions at the sediment

15 surface, consequently reducing the oxygen penetration depth and hence increasing benthic dFe fluxes (Elrod et al., 2004). However, reductive mobilization of iron from the sediments is only one of the mechanisms believed to introduce dFe to the ocean interior. At the sediment–water interface, in fact, the remineralisation of sediments resuspended by bottom or tidal currents (Young et al., 2011; Blain et al., 2008), internal

20 wave's activity (Blain et al., 2008) or wind-induced wave-action (Gargett et al., 2004; de Jong et al., 2012) can introduce additional dFe to the water column.

The total amount of dFe that ultimately leaves the bottom layer towards the surface depends on multiple concomitant factors, including the magnitude of bottom friction resuspending sediment particles, oxygen concentrations in the bottom water, the

25 concentration and type of organic ligands actively stabilizing dFe, or the presence of dFe-scavenging particles settling to the bottom (de Jong et al., 2012; Klunder et al., 2011). Once dFe (in free inorganic or ligand-complexed form) leaves the bottom layer closer to the sediment–water interface, the combination of diffusion and vertical advection brings dFe to the surface where lateral transport distributes it in the region. Of

the three mentioned processes, previous studies in the Southern Ocean (i.e., de Jong et al., 2012; Planquette et al., 2007) agree that lateral advection is the most important and efficient long-distance supplier of dFe (see also Lam et al., 2006). The importance of lateral transport around South Georgia has been suggested by several authors (i.e., Korb et al., 2008) and is evident from our modelling results (Fig. 8a).

Whitehouse et al. (2008a) and Nielsdóttir et al. (2012) point also to upwelling to the southwest of the island or in relation to eddies. Our sensitivity runs suggest that only a very small part of the total dFe measured at the surface derives from upwelling of deeper iron-rich waters. However, as noted previously, the lack of tidal forcing and the coarse grid resolution used in the modelling experiments presented here will not allow a full representation of vertical processes acting at the meso and sub-mesoscale or in relation to the presence of eddies and tides, better represented by higher resolution models (Naveira Garabato et al., 2002; Young et al., 2011).

At the surface the main mechanisms removing dFe are likely to be biological uptake by phytoplankton and bacteria, scavenging onto sinking biogenic particles (i.e., dead phytoplankton cells), oxidation of dFe and its adsorption to colloids. However, the high surface dFe concentrations measured around South Georgia, which result from the combination of all processes mentioned above, clearly indicate that dFe sources are far more effective than dFe losses. In fact, Borrione and Schlitzer (2013) suggest that the termination of the first peak observed in South Georgia phytoplankton blooms does not strictly depend on dFe availability, but rather it may be caused by insufficient silicate levels, rapidly exhausted by the spring and early summer phytoplankton blooms.

Iron-input mechanisms directly related to local hydrography, like lateral transport or tidal currents, are not expected to change significantly in time (i.e., at the seasonal or decadal scale), especially if they are steered by bottom topography (Borrione and Schlitzer, 2013). Conversely, iron-input mechanisms directly linked to weather or local climate (i.e., air temperature or precipitation) will likely follow a seasonal cycle, and possibly be modified in the future as a response to climate change. For example, during austral summer dust emission from the Patagonian desert and snow and ice-melt

Title Page

Abstract | Introduction

Conclusions | References

Tables | Figures

⏮ | ⏭

◀ | ▶

Back | Close

Full Screen / Esc

Printer-friendly Version

Interactive Discussion

are at their maximum levels and hence coincide in timing with the main phytoplankton growing season (Johnson et al., 2010; Young et al., 2011; Borrione and Schlitzer, 2013): during this time of the year the growing and iron-demanding phytoplankton community can count on an additional exogenous source of iron other than the continuous supply of iron from sedimentary sources. An increase in dFe input can be expected at the longer time-scales due to the gradual but progressive increase in ocean and air temperatures which are leading to increased glacier melt (Gordon et al., 2008; Whitehouse et al., 2008b). Previous studies investigating the magnitude of climate-change induced dust emission and deposition from the world's deserts, provide contrasting results, depending on the models and initial scenarios used (Mahowald and Luo, 2003; Tegen et al., 2004). However, considering the stronger effect of sedimentary versus atmospheric sources of iron to the main South Georgia bloom area revealed by the current study, we suggest that either an increase or decrease in future dust deposition, will have a negligible effect on primary productivity (see also Tagliabue et al., 2008; Aumont et al., 2008).

5.3   Model uncertainties

Comparison of modelled surface dFe concentrations with recently published underway dFe concentrations measured around South Georgia (Figs. 7a and 8a) reconfirm the ability of PISCES (here coupled to ROMS_AGRIF) to reproduce the main distribution features of surface dFe, and, to an adequate level also absolute dFe concentrations. Results shown in Fig. 6 indicate that patterns in simulated and observed surface Chl *a* concentrations have many similarities because in both datasets location and size of the blooms clearly depend on local circulation, which is also reproduced adequately by the model. However, modelled and observed Chl *a* concentrations are significantly different in their absolute values: modelled Chl *a* concentrations are lower than those observed in January–February 2008, but also lower than the concentrations recorded during the less productive months of January–February 2011. Significant differences between the

two datasets indicate that in the current configuration of PISCES applied to the region around South Georgia, certain biogeochemical processes may not be fully resolved.

The first important difficulty encountered in biogeochemical models applied to the iron-limited Southern Ocean, is the correct representation of the complex iron cycle, necessarily simplified because of the large number of uncertainties and limited number of observations (Aumont and Bopp, 2006). Observations in fact have shown that in seawater, iron is present in various oxidation forms, and that it interacts with several types and size classes of particles and ligands. In the current configuration of PISCES, iron is present in dissolved form and it is assumed to be all bioavailable (as in Moore and Braucher, 2008); moreover, in the model dFe may interact with biogenic particles only. Although recent investigations indicated the ubiquity of inorganic particulate iron, especially downstream of coastal regions (i.e., Lam et al., 2006), but also suggested its bioavailability (i.e., Raiswell et al., 2008), the inorganic form of particulate iron is currently not included in the model, as almost no quantitative information is available to parametrize this source (Aumont and Bopp, 2006). Furthermore, recent studies show that the concentration of ligands, which are responsible for the stabilization and hence prolonged bioavailability of dFe in the water column, is very variable in space, time and depth; in particular, ligands are present at higher concentrations where productivity is high (Hunter and Boyd, 2007; Moore and Braucher, 2008), as would likely be the case over the South Georgia main bloom area. In the model however, there is only one type of ligands, and they are present at constant concentrations throughout the whole water-column. Consequently, an underestimate of the total concentration of bioavailable iron, which is potentially also present in the form of inorganic particulate iron, or complexed to higher concentrations of ligands, may result in the low modelled Chl a concentrations. To date, there are no in situ measurements around South Georgia that could help better ascertain the role of particulate iron in the region, including its bioavailability and transport scale lengths. These measurements are fundamental to confirm or reject our hypothesis.

The lifetime of iron in the surface layer depends on the interaction between chemical, physical and biological processes removing or reintroducing iron. As mentioned above the presence of ligands is crucial to keep iron dissolved in seawater (Hunter and Boyd, 2007), while diffusion, as well as lateral and vertical mixing or advection (Fig. 10) provide the means for iron supply from more enriched waters. Indeed, also the biological recycling of iron, due to phytoplankton, zooplankton and bacteria, will sensibly increase the lifetime of iron in the surface. Although these processes are represented in the model (Fig. 3), their relative importance may be affected by uncertainties in the rates of biological iron uptake, chemical processing, and its release into the water-column (Baker et al., 2010).

6 Conclusions

Natural input of iron around South Georgia, was investigated using the coupled physical-biogeochemical model ROMS_AGRIF-PISCES, implemented for the first time to a region of the Southern Ocean. The model captures the main features of circulation and primary productivity around the island, providing new evidence for the South Georgia island mass effect. In particular, the model can reproduce surface dFe distributions previously described with few discrete in situ measurements around South Georgia, and hence presents a large scale, yet detailed view of iron distribution, scale lengths and principal transport pathways around the island. To date this information was absent, and can now offer a useful tool to biogeochemists investigating the occurrence of phytoplankton blooms in the region but can also provide a base line for future in situ investigations. Clearly, some important questions remain open. Although the model captures adequately the overall distribution and magnitude of dFe distribution in the region as well as the main spatial patterns of phytoplankton blooms, modelled Chl *a* concentrations are significantly lower than in observations. This evident discrepancy may suggest that the total amount of iron bioavailable to phytoplankton, includes but is not limited to dFe, and that recycling processes may be more efficient than currently

simulated. Both aspects need to be verified by future investigations. In the mean time, as the model used in this study has proven its ability to simulate the South Georgia island mass effect in HNLC waters, additional model sensitivity tests could be performed in the future to estimate which levels of bioavailable iron are necessary to stimulate the particularly intense annual phytoplankton blooms observed downstream of South Georgia.

References

Ardelan, M. V., Holm-Hansen, O., Hewes, C. D., Reiss, C. S., Silva, N. S., Dulaiova, H., Steinnes, E., and Sakshaug, E.: Natural iron enrichment around the Antarctic Peninsula in the Southern Ocean, Biogeosciences, 7, 11–25, doi:10.5194/bg-7-11-2010, 2010.

Aumont, O. and Bopp, L.: Globalizing results from ocean in situ iron fertilization studies, Global Biogeochem. Cy., 20, GB2017, doi:10.1029/2005GB002591, 2006.

Aumont, O., Maier-Reimer, E., Blain, S., and Monfray, P.: An ecosystem model of the global ocean including Fe, Si, P colimitations, Global Biogeochem. Cy., 17, 1060, doi:10.1029/2001GB001745, 2003.

Aumont, O., Bopp, L., and Schulz, M.: What does temporal variability in aeolian dust deposition contribute to sea-surface iron and chlorophyll distributions?, Geophys. Res. Lett., 35, L07607, doi:10.1029/2007gl031131, 2008.

Baker, A. R. and Croot, P. L.: Atmospheric and marine controls on aerosol iron solubility in seawater, Mar. Chem., 120, 4–13, doi:10.1016/j.marchem.2008.09.003, 2010.

Beckmann, A. and Haidvogel, D. B.: Numerical simulation of flow around a tall isolated seamount. Part I: Problem formulation and model accuracy, J. Phys. Oceanogr., 23, 1736–1753, doi:10.1175/1520-0485(1993)023<1736:NSOFAA>2.0.CO;2, 1993.

Blain, S., Sarthou, G., and Laan, P.: Distribution of dissolved iron during the natural iron-fertilization experiment KEOPS (Kerguelen Plateau, Southern Ocean), Deep-Sea Res. Pt. II, 55, 594–605, doi:10.1016/j.dsr2.2007.12.028, 2008.

Borrione, I. and Schlitzer, R.: Distribution and recurrence of phytoplankton blooms around South Georgia, Southern Ocean, Biogeosciences, 10, 217–231, doi:10.5194/bg-10-217-2013, 2013.

Bucciarelli, E., Blain, S., and Tréguer, P.: Iron and manganese in the wake of the Kerguelen Islands (Southern Ocean), Mar. Chem., 73, 21–36, doi:10.1016/S0304-4203(00)00070-0, 2001.

Carton, J. A. and Giese, B. S.: A Reanalysis of Ocean Climate Using Simple Ocean Data Assimilation (SODA), Mon. Weather Rev., 136, 2999–3017, doi:10.1175/2007mwr1978.1, 2008.

Casey, K. S. and Cornillon, P.: A comparison of satellite and in situ-based sea surface temperature climatologies, J. Climate, 12, 1848–1863, doi:10.1175/1520-0442(1999)012<1848:acosai>2.0.co;2, 1999.

Conkright, M. E., Locarnini, R. A., Garcia, H. E., O'Brien, T. D., Boyer, T. P., Stephens, C., and Antonov, J. I.: World Ocean Atlas 2001: Objective Analyses, Data Statistics, and Figures, CD-ROM Documentation, National Oceanographic Data Center, Silver Spring, MD, 17 pp., 2002.

Da Silva, A. M., Young, C. C., and Levitus, S.: Atlas of Surface Marine Data 1994, vol. 1, Algorithms and Procedures, NOAA Atlas NESDIS 6, US Department of Commerce, NOAA, NESDIS, USA, 74 pp., 1994.

Debreu, L. and Blayo, E.: Two-way embedding algorithms: a review, Ocean Dynam., 58, 415–428, doi:10.1007/s10236-008-0150-9, 2008.

de Jong, J., Schoemann, V., Lannuzel, D., Croot, P., de Baar, H., and Tison, J.-L.: Natural iron fertilization of the Atlantic sector of the Southern Ocean by continental shelf sources of the Antarctic Peninsula, J. Geophys. Res., 117, G01029, doi:10.1029/2011jg001679, 2012.

Title Page

Abstract | Introduction

Conclusions | References

Tables | Figures

◄ | ►

◄ | ►

Back | Close

Full Screen / Esc

Printer-friendly Version

Interactive Discussion

Elrod, V. A., Berelson, W. M., Coale, K. H., and Johnson, K. S.: The flux of iron from continental shelf sediments: a missing source for global budgets, Geophys. Res. Lett., 31, L12307, doi:10.1029/2004gl020216, 2004.

Gargett, A., Wells, J., Tejada-Martínez, A. E., and Grosch, C. E.: Langmuir supercells: a mechanism for sediment resuspension and transport in shallow seas, Science, 306, 1925–1928, doi:10.1126/science.1100849, 2004.

Ginoux, P., Chin, M., Tegen, I., Prospero, J. M., Holben, B., Dubovik, O., and Lin, S.-J.: Sources and distributions of dust aerosols simulated with the GOCART model, J. Geophys. Res.-Atmos., 106, 20255–20273, doi:10.1029/2000jd000053, 2001.

Gordon, J. E., Haynes, V. M., and Hubbard, A.: Recent glacier changes and climate trends on South Georgia, Global Planet. Change, 60, 72–84, doi:10.1016/j.gloplacha.2006.07.037, 2008.

Holeton, C., Nédélec, F., Sanders, R., Brown, L., Moore, C., Stevens, D., Heywood, K., Statham, P., and Lucas, C.: Physiological state of phytoplankton communities in the Southwest Atlantic sector of the Southern Ocean, as measured by fast repetition rate fluorometry, Polar Biol., 29, 44–52, doi:10.1007/s00300-005-0028-y, 2005.

Hunter, K. A. and Boyd, P. W.: Iron-binding ligands and their role in the ocean biogeochemistry of iron, Environ. Chem., 4, 221–232, doi:10.1071/EN07012, 2007.

Johnson, K. S., Gordon, R. M., and Coale, K. H.: What controls dissolved iron concentrations in the world ocean?, Mar. Chem., 57, 137–161, doi:10.1016/S0304-4203(97)00043-1, 1997.

Johnson, M. S., Meskhidze, N., Solmon, F., Gassó, S., Chuang, P. Y., Gaiero, D. M., Yantosca, R. M., Wu, S., Wang, Y., and Carouge, C.: Modeling dust and soluble iron deposition to the South Atlantic Ocean, J. Geophys. Res., 115, D15202, doi:10.1029/2009jd013311, 2010.

Jones, E. M., Bakker, D. C. E., Venables, H. J., and Watson, A. J.: Dynamic seasonal cycling of inorganic carbon downstream of South Georgia, Southern Ocean, Deep-Sea Res. Pt. II, 59–60, 25–35, doi:10.1016/j.dsr2.2011.08.001, 2012.

Karakas, G., Nowald, N., Blaas, M., Marchesiello, P., Frickenhaus, S., Schlitzer, R.: High-resolution modeling of sediment erosion and particle transport across the northwest African shelf, J. Geophys. Res., 111, C06025, doi:10.1029/2005jc003296, 2006.

Klunder, M. B., Laan, P., Middag, R., De Baar, H. J. W., and van Ooijen, J. C.: Dissolved iron in the Southern Ocean (Atlantic sector), Deep-Sea Res. Pt. II, 58, 2678–2694, doi:10.1016/j.dsr2.2010.10.042, 2011.

Korb, R. E. and Whitehouse, M.: Contrasting primary production regimes around South Georgia, Southern Ocean: large blooms versus high nutrient, low chlorophyll waters, Deep-Sea Res. Pt. I, 51, 721–738, doi:10.1016/j.dsr.2004.02.006, 2004.

Korb, R. E., Whitehouse, M. J., and Ward, P.: SeaWiFS in the southern ocean: spatial and temporal variability in phytoplankton biomass around South Georgia, Deep-Sea Res. Pt. II, 51, 99–116, doi:10.1016/j.dsr2.2003.04.002, 2004.

Korb, R. E., Whitehouse, M. J., Atkinson, A., and Thorpe, S. E.: Magnitude and maintenance of the phytoplankton bloom at South Georgia: a naturally iron-replete environment, Mar. Ecol.-Prog. Ser., 368, 75–91, doi:10.3354/meps07525, 2008.

Lam, P. J., Bishop, J. K. B., Henning, C. C., Marcus, M. A., Waychunas, G. A., and Fung, I. Y.: Wintertime phytoplankton bloom in the subarctic Pacific supported by continental margin iron, Global Biogeochem. Cy., 20, GB1006, doi:10.1029/2005gb002557, 2006.

Mahowald, N. M. and Luo, C.: A less dusty future?, Geophys. Res. Lett., 30, 1903, doi:10.1029/2003gl017880, 2003.

Mahowald, N. M., Baker, A. R., Bergametti, G., Brooks, N., Duce, R. A., Jickells, T. D., Kubilay, N., Prospero, J. M., and Tegen, I.: Atmospheric global dust cycle and iron inputs to the ocean, Global Biogeochem. Cy., 19, GB4025, doi:10.1029/2004gb002402, 2005.

Meskhidze, N., Nenes, A., Chameides, W. L., Luo, C., and Mahowald, N.: Atlantic Southern Ocean productivity: fertilization from above or below?, Global Biogeochem. Cy, 21, GB2006, doi:10.1029/2006gb002711, 2007.

Middelburg, J. J., Soetaert, K., Herman, P. M. J., and Heip, C. H. R.: Denitrification in marine sediments: a model study, Global Biogeochem. Cy., 10, 661–673, doi:10.1029/96gb02562, 1996.

Moore, J. K. and Braucher, O.: Sedimentary and mineral dust sources of dissolved iron to the world ocean, Biogeosciences, 5, 631–656, doi:10.5194/bg-5-631-2008, 2008.

Moore, J. K., Abbott, M. R., and Richman, J. G.: Location and dynamics of the Antarctic Polar Front from satellite sea surface temperature data, J. Geophys. Res., 104, 3059–3073, doi:10.1029/1998jc900032, 1999.

Naveira Garabato, A. C., Strass, V. H., and Kattner, G.: Fluxes of nutrients in a three-dimensional meander structure of the Antarctic Polar Front, Deep-Sea Res. Pt. II, 49, 3771–3792, doi:10.1016/S0967-0645(02)00110-8, 2002.

Title Page

Abstract | Introduction

Conclusions | References

Tables | Figures

◄◄ | ►►

◄ | ►

Back | Close

Full Screen / Esc

Printer-friendly Version

Interactive Discussion

Nielsdóttir, M. C., Bibby, T. S., Moore, C. M., Hinz, D. J., Sanders, R., Whitehouse, M., Korb, R., and Achterberg, E. P.: Seasonal and spatial dynamics of iron availability in the Scotia Sea, Mar. Chem., 130–131, 62–72, doi:10.1016/j.marchem.2011.12.004, 2012.

Orsi, A. H., Whitworth, T., and Nowlin, W. D.: On the meridional extent and fronts of the Antarctic Circumpolar Current, Deep-Sea Res. Pt. I, 42, 641–673, doi:10.1016/0967-0637(95)00021-W, 1995.

Parekh, P., Follows, M. J., and Boyle, E.: Modeling the global ocean iron cycle, Global Biogeochem. Cy., 18, GB1002, doi:10.1029/2003GB002061, 2004.

Penven, P., Debreu, L., Marchesiello, P., and McWilliams, J. C.: Evaluation and application of the ROMS 1-way embedding procedure to the central california upwelling system, Ocean Model., 12, 157–187, doi:10.1016/j.ocemod.2005.05.002, 2006.

Penven, P., Marchesiello, P., Debreu, L., and Lefèvre, J.: Software tools for pre- and post-processing of oceanic regional simulations, Environ. Modell. Softw., 23, 660–662, doi:10.1016/j.envsoft.2007.07.004, 2008.

Planquette, H., Statham, P. J., Fones, G. R., Charette, M. A., Moore, C. M., Salter, I., Nédélec, F. H., Taylor, S. L., French, M., Baker, A. R., Mahowald, N., and Jickells, T. D.: Dissolved iron in the vicinity of the Crozet Islands, Southern Ocean, Deep-Sea Res. Pt. II, 54, 1999–2019, doi:10.1016/j.dsr2.2007.06.019, 2007.

Raiswell, R., Benning, L. G., Davidson, L., and Tranter, M.: Nanoparticulate bioavailable iron minerals in icebergs and glaciers, Mineral. Mag., 72, 345–348, doi:10.1180/minmag.2008.072.1.345, 2008.

Shchepetkin, A. F. and McWilliams, J. C.: The regional oceanic modeling system (ROMS): a split-explicit, free-surface, topography-following-coordinate oceanic model, Ocean Model., 9, 347–404, doi:10.1016/j.ocemod.2004.08.002, 2005.

Ridgway, K. R., Dunn, J. R., and Wilkin, J. L.: Ocean interpolation by four-dimensional least squares-application to the waters around Australia, J. Atmos. Ocean. Tech., 19, 1357–1375, 2002.

Slemons, L., Gorgues, T., Aumont, O., Menkes, C., and Murray, J. W.: Biogeochemical impact of a model western iron source in the Pacific Equatorial Undercurrent, Deep-Sea Res. Pt. I, 56, 2115–2128, doi:10.1016/j.dsr.2009.08.005, 2009.

Smith, W. H. F. and Sandwell, D. T.: Global sea floor topography from satellite altimetry and ship depth soundings, Science, 277, 1956–1962, doi:10.1126/science.277.5334.1956, 1997.

Tagliabue, A., Bopp, L., and Aumont, O.: Ocean biogeochemistry exhibits contrasting responses to a large scale reduction in dust deposition, Biogeosciences, 5, 11–24, doi:10.5194/bg-5-11-2008, 2008.

Tagliabue, A., Bopp, L., and Aumont, O.: Evaluating the importance of atmospheric and sedimentary iron sources to Southern Ocean biogeochemistry, Geophys. Res. Lett., 36, L13601, doi:10.1029/2009gl038914, 2009.

Tegen, I. and Fung, I.: Contribution to the atmospheric mineral aerosol load from land surface modification, J. Geophys. Res.-Atmos., 100, 18707–18726, doi:10.1029/95jd02051, 1995.

Tegen, I., Werner, M., Harrison, S. P., and Kohfeld, K. E.: Relative importance of climate and land use in determining present and future global soil dust emission, Geophys. Res. Lett., 31, L05105, doi:10.1029/2003gl019216, 2004.

Thorpe, S. E., Heywood, K. J., Brandon, M. A., and Stevens, D. P.: Variability of the southern Antarctic Circumpolar Current front north of South Georgia, J. Marine Syst., 37, 87–105, doi:10.1016/S0924-7963(02)00197-5, 2002.

Venables, H., Meredith, M. P., Atkinson, A., and Ward, P.: Fronts and habitat zones in the Scotia Sea, Deep-Sea Res. Pt. II, 59–60, 14–24, doi:10.1016/j.dsr2.2011.08.012, 2012.

Ward, P., Shreeve, R., Whitehouse, M., Korb, B., Atkinson, A., Meredith, M., Pond, D., Watkins, J., Goss, C., and Cunningham, N.: Phyto- and zooplankton community structure and production around South Georgia (Southern Ocean) during Summer 2001/02, Deep-Sea Res. Pt. I, 52, 421–441, doi:10.1016/j.dsr.2004.10.003, 2005.

Whitehouse, M. J., Priddle, J., and Symon, C.: Seasonal and annual change in seawater temperature, salinity, nutrient and chlorophyll *a* distributions around South Georgia, South Atlantic, Deep-Sea Res. Pt. I, 43, 425–443, doi:10.1016/0967-0637(96)00020-9, 1996.

Whitehouse, M. J., Korb, R. E., Atkinson, A., Thorpe, S. E., and Gordon, M.: Formation, transport and decay of an intense phytoplankton bloom within the high-nutrient low-chlorophyll belt of the Southern Ocean, J. Marine Syst., 70, 150–167, doi:10.1016/j.jmarsys.2007.05.003, 2008a.

Whitehouse, M. J., Meredith, M. P., Rothery, P., Atkinson, A., Ward, P., and Korb, R. E.: Rapid warming of the ocean around South Georgia, Southern Ocean, during the 20th century: forcings, characteristics and implications for lower trophic levels, Deep-Sea Res. Pt. I, 55, 1218–1228, doi:10.1016/j.dsr.2008.06.002, 2008b.

Young, E. F., Meredith, M. P., Murphy, E. J., and Carvalho, G. R.: High-resolution modelling of the shelf and open ocean adjacent to South Georgia, Southern Ocean, Deep-Sea Res. Pt. II, 58, 1540–1552, doi:10.1016/j.dsr2.2009.11.003, 2011.

Table 1. Averages of surface dFe and Chl *a* concentrations from each sensitivity run and from the domain around South Georgia depicted in Fig. 7a. RMS and mean differences between each sensitivity run and the SEDDUST scenario are also indicated.

Name of scenario	Average ± std (nM 10^{-1} dFe)	Average ± std (mg Chl *a* m^{-3})	RMS/mean diff. (nM dFe)	RMS/mean diff. (mg Chl *a* m^{-3})
SEDDUST[a]	1.98 ± 6.01	0.33 ± 0.28	/	/
SED_NODUST	1.92 ± 5.90	0.31 ± 0.29	0.01/−0.01	0.02/−0.02
NOSED_DUST[a]	0.25 ± 0.05	0.15 ± 0.02	0.62/−0.18	0.33/−0.18
SEDDUST_0–5 m[a]	0.82 ± 2.32	0.25 ± 0.22	0.39/−0.12	0.14/−0.09
SEDDUST_5–10 m[a]	0.42 ± 0.84	0.2 ± 0.14	0.54/−0.15	0.23/−0.14
SEDDUST_10–15 m	0.35 ± 0.51	0.18 ± 0.1	0.57/−0.16	0.26/−0.15
SEDDUST_15–20 m[a]	0.32 ± 0.38	0.17 ± 0.08	0.58/−0.17	0.28/−1.58
SEDDUST_20–25 m	0.30 ± 0.31	0.17 ± 0.07	0.59/−0.17	0.29/−0.16
SEDDUST_25–30 m	0.3 ± 0.28	0.17 ± 0.06	0.6/−0.17	0.3/−0.16
SEDDUST_50–55 m	0.26 ± 0.10	0.16 ± 0.03	0.61/−0.17	0.32/−0.17
SEDDUST_100–105 m[a]	0.25 ± 0.05	0.15 ± 0.03	0.62/−0.17	0.33/−0.18
SEDDUST_100–105 m[b]	0.25 ± 0.05	0.15 ± 0.03	0.001/∼ 0	0.002/0.001

[a] Surface (0–30 m) averages of dFe and Chl *a* for these simulations are shown in Fig. 9.
[b] RMS and mean-differences are calculated with respect to the NOSED_DUST simulation.
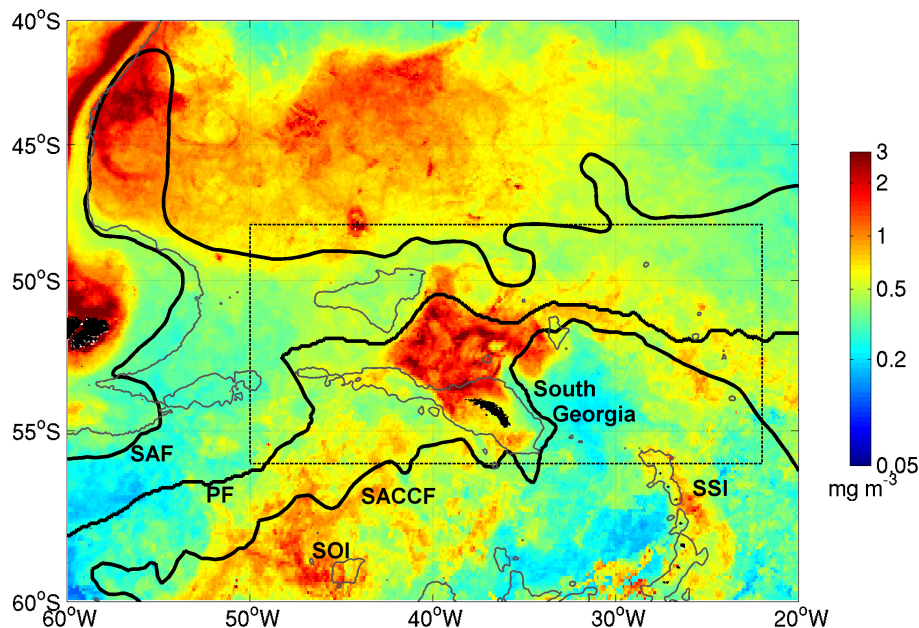
Fig. 1. Austral summer (January–February) chlorophyll *a* climatology derived from MODIS for the 2006–2011 time-period in the southwestern sector of the Atlantic Southern Ocean. Bold lines indicate the Subantarctic Front (SAF, Orsi et al., 1995), the Polar Front (PF, Moore et al., 1999) and the Southern ACC Front (SACCF, Thorpe et al., 2002). The position of the South Orkney Islands (SOI) and the South Sandwich Islands (SSI) are also indicated. The rectangle indicates the South Georgia area mentioned in the text.
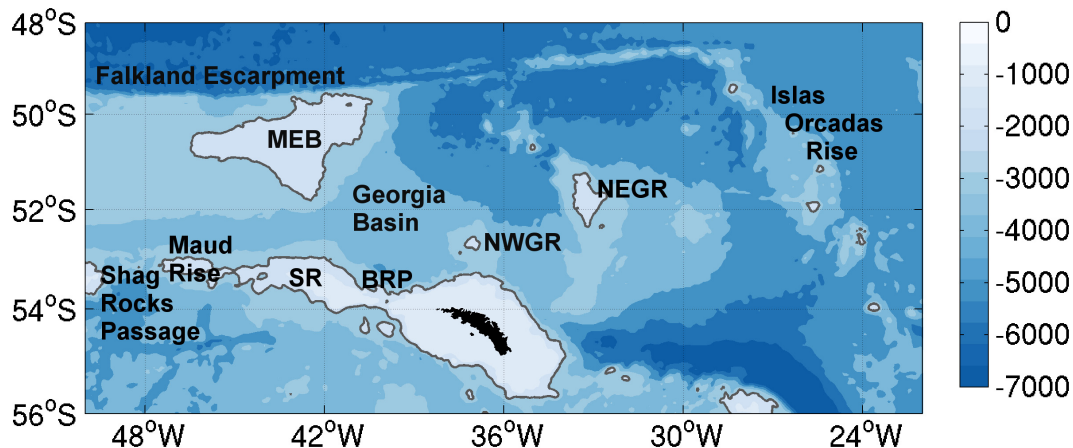
Fig. 2. Bathymetry and main topographic features in the South Georgia area: MEB: Maurice Ewing Bank; SR: Shag Rocks; BRP: Black Rocks Passage; NWGR: North West Georgia Rise; NEGR: North East Georgia Rise. Bathymetric contours for the 2000 m are indicated with thin lines.

Full Screen / Esc

Printer-friendly Version

Interactive Discussion
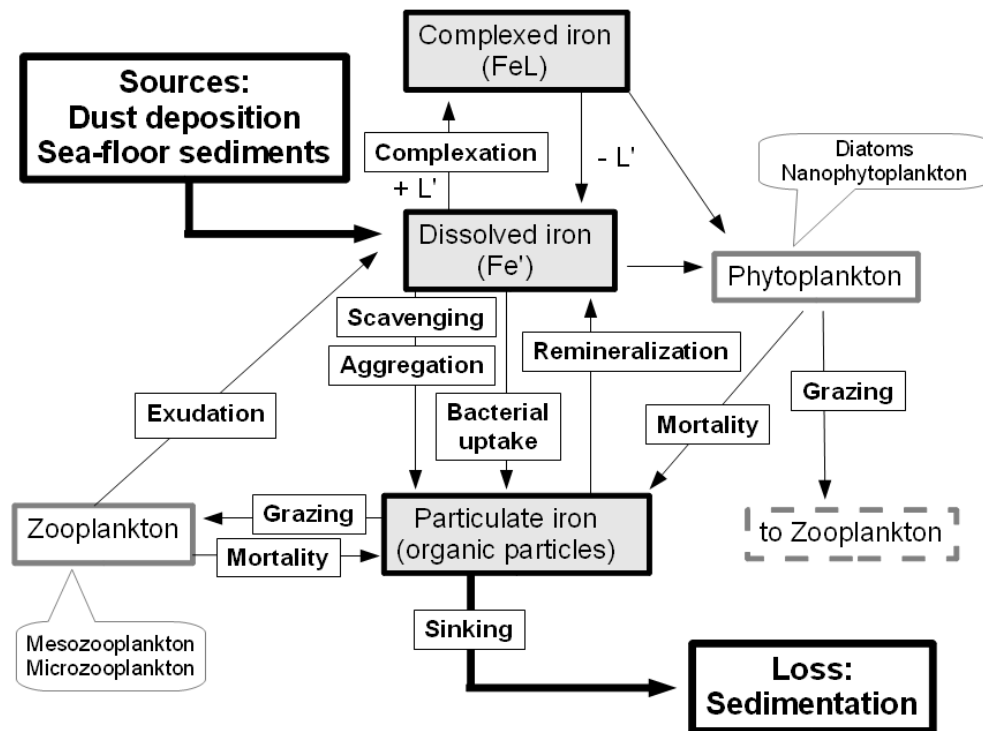
Fig. 3. Schematics of the iron cycle in PISCES as implemented in the current application (modified from Slemons et al., 2009). Fe′ indicates free inorganic dissolved iron, L′ are ligands, while FeL indicates dissolved iron complexed to ligands.
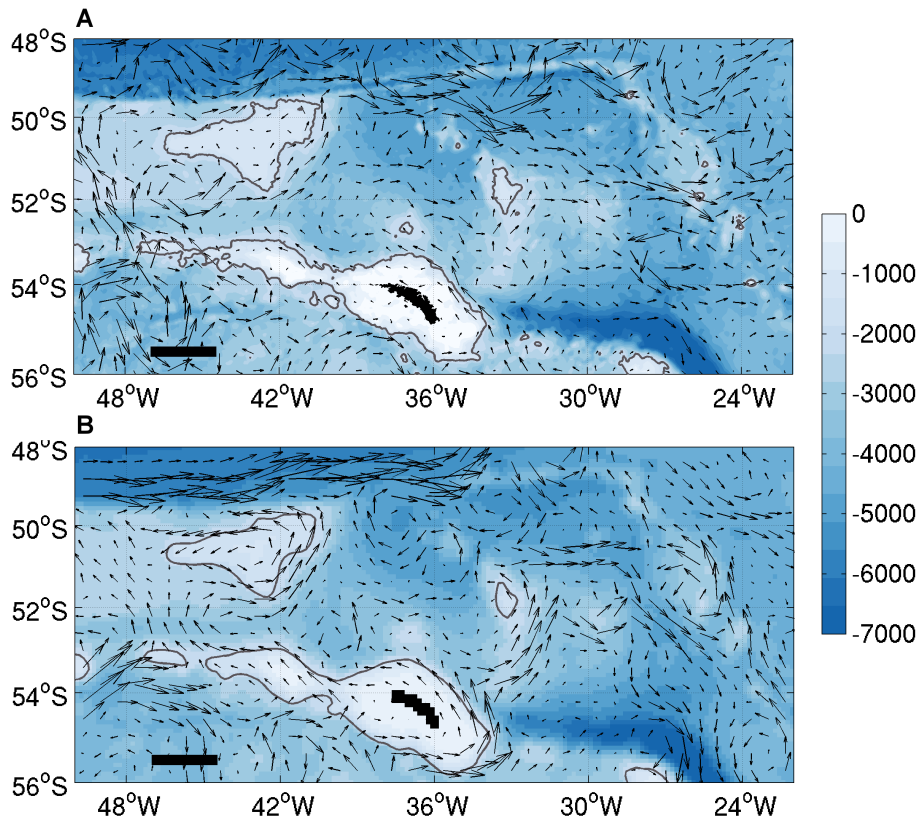
Fig. 4. Surface circulation (black arrows) in the South Georgia area, as obtained from **(A)** Aviso satellite altimetry for January–February 2008 and from **(B)** model results for January–February of the last modelling year. Background colours indicate bottom topography. For reference, the 2000 m bathymetry is indicated with thin grey lines. In both panels, the horizontal bar in the bottom-left corner indicates $1\,\mathrm{m\,s^{-1}}$, and corresponds to approximately 160 km. Modelled surface circulation is interpolated onto the coarser grid resolution of satellite altimetry.

Title Page

Abstract | Introduction

Conclusions | References

Tables | Figures

|◄ | ►|

◄ | ►

Back | Close

Full Screen / Esc
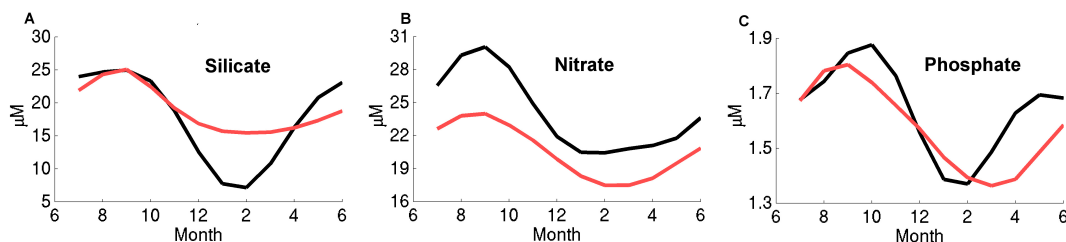
Fig. 5. Annual cycles of surface (0–30 m) silicate **(A)**, nitrate **(B)** and phosphate concentrations averaged over the South Georgia domain defined between 45–32° W and 56–50° S (shown in Fig. 7a) from the CARS2009 climatology (black lines) and from model outputs from the last modelling year of the SEDDUST scenario (red line).
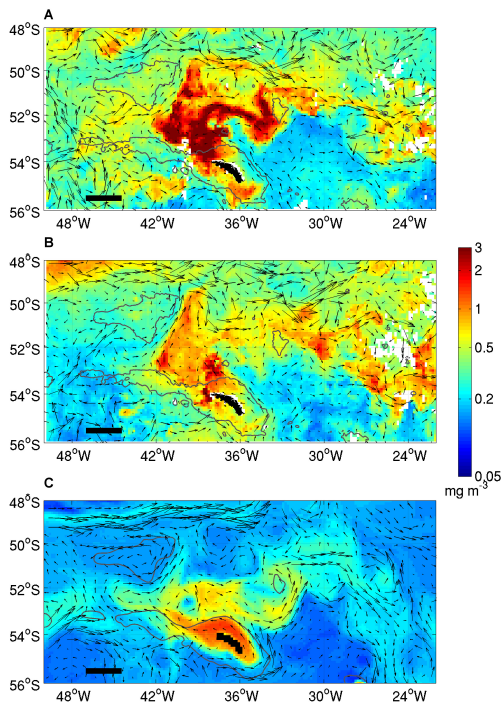
Fig. 6. Surface Chl *a* concentrations in the South Georgia area as obtained from MODIS ocean colour estimates for January–February 2008 **(A)** and January–February 2011 **(B)**. Satellite estimates are interpolated onto the model's coarser grid resolution. In **(C)** surface (0–30 m) averages of Chl *a* concentrations from January–February of the last modelling year. In all cases, black arrows report contemporaneous surface circulation patterns either from Aviso altimetry (in **A** and **B**) or from the model (in **C**). Circulation patterns in (**A** and **C**) are equivalent to those depicted in Fig. 4. In all panels the 2000 m bathymetry is indicated with thin grey lines; the horizontal bar in the bottom-left corner indicates $1\,\mathrm{m\,s^{-1}}$, and corresponds to approximately 160 km.
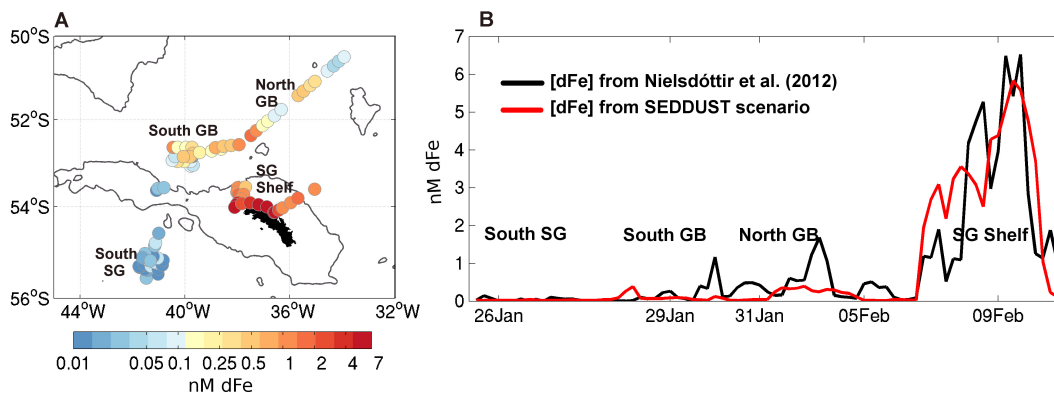
Fig. 7. (A) Locations and concentrations of dFe underway measurement from January and February of 2008 (Nielsdóttir et al., 2012). **(B)** Underway measurements of dFe (black line) and simulated surface dFe concentrations (red line); model values were interpolated onto the dFe sampling locations shown in **(A)**. For reference, the x-axis indicates dates of in situ dFe sampling. The main geographical areas are also indicated, and correspond to those marked in **(A)**.
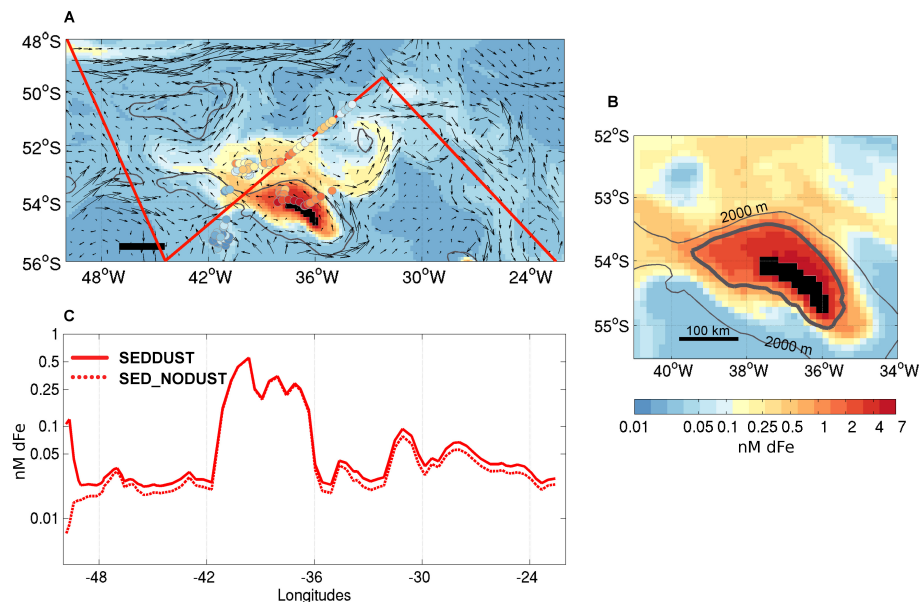
Fig. 8. Simulated surface (0–30 m) dFe concentrations for January–February of the last modelling year. In **(A)** dFe concentrations (colour-scale as in **B**) are obtained from the SEDDUST scenario; coloured dots indicate in situ surface dFe concentrations measured by Nielsdóttir et al. (2012), shown also in Fig. 7a. The red line marks a virtual transect along which are extracted modelled dFe concentrations depicted in **(C)**; black arrows represent the contemporaneous surface circulation as depicted in Fig. 4b; the horizontal bar indicates $1\,\mathrm{m\,s^{-1}}$ and corresponds to approximately 160 km. **(B)** dFe concentrations from the SEDDUST scenario (detail from panel **A**); the thick contour line indicates dFe concentrations equal to 1.35 nM, here marked to estimate dFe scale lengths; see text for more details. **(C)** modelled dFe concentrations for points along the red line drawn in **(A)**. Solid line depicts values obtained from the SEDDUST scenario (i.e., including sedimentary and atmospheric deposition of dFe), dashed line depicts dFe values obtained from the SED_NODUST scenario where there is no atmospheric deposition of dFe.

Title Page

Abstract | Introduction

Conclusions | References

Tables | Figures

|◄ | ►|

◄ | ►

Back | Close

Full Screen / Esc

Printer-friendly Version
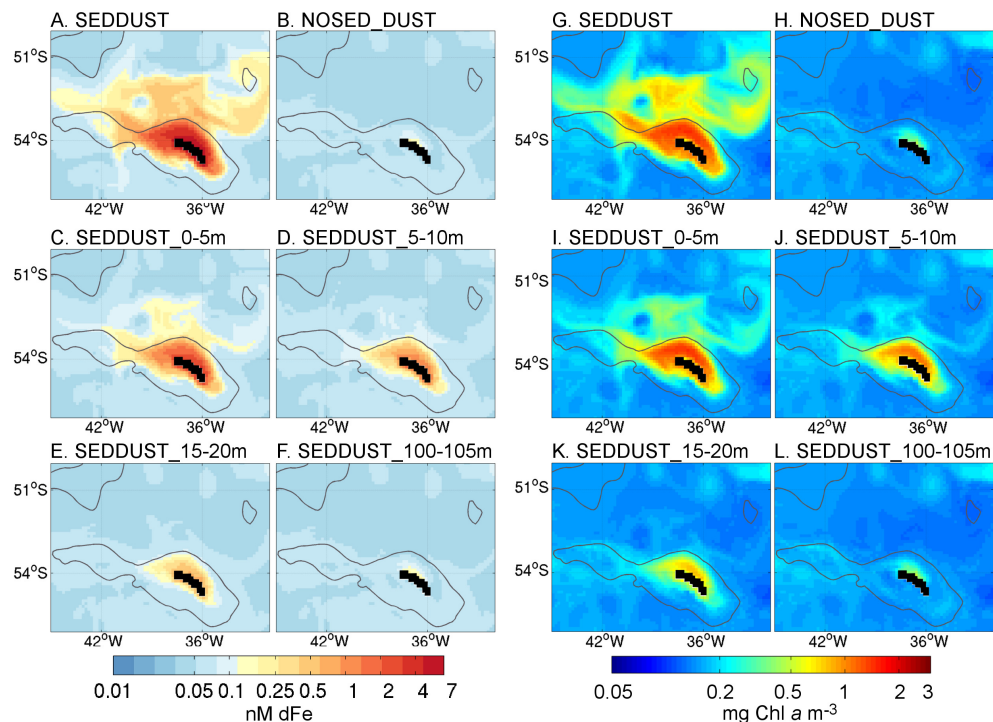
Interactive Discussion

Fig. 9. Surface (0–30 m) dFe concentrations (**A–J** on the left) and Chl *a* concentrations (**G–L** on the right) for January–February of the last modelling year obtained with simulations including different sedimentary sources of iron. Results for the reference runs (i.e., SEDDUST and NOSED_DUST) are shown in the first row. See also Table 1 and Sect. 2.3 for further details on each simulation.

Title Page

Abstract · Introduction

Conclusions · References

Tables · Figures

|◀ · ▶|

◀ · ▶

Back · Close

Full Screen / Esc
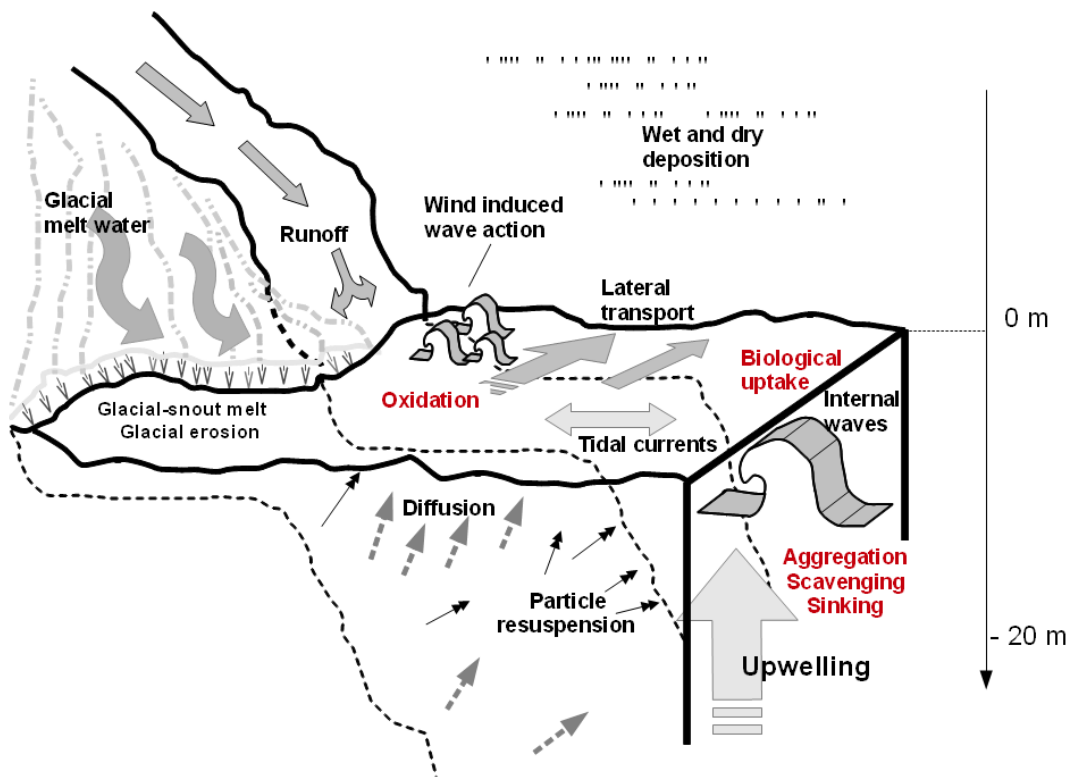
Printer-friendly Version

Interactive Discussion

Fig. 10. Schematic overview of the potential coastal and shelf processes leading to the surface distribution of dFe observed around South Georgia (i.e., Fig. 8). Processes removing dFe from the water column are indicated in red.